PAPER

Check for updates

Innovative electrospun macromolecule-based nanofibers for cationic dye removal and antibacterial applications

Reem Fathy, [ab] A. M. Abdelghany, [c] Wael I. Mortada [ID] *[d] and E. Abdel-Latif[a]

A novel nanocomposite fiber membrane, made from polycaprolactone (PCL), barium titanate (BT), and sodium lauryl sulfate (SLS), was prepared and investigated for its methylene blue (MB) adsorption properties and for antibacterial activity. The nanofibers (SLS-PCL/BT) were fabricated *via* electrospinning and characterized using SEM, FTIR, AFM, and contact angle measurements. Batch adsorption tests assessed the effects of pH, contact time, sorbent dose, initial dye concentration, temperature, and salt concentration. The maximum uptake of MB uptake was achieved at pH 12, sorbent dose of 60 mg, and 180 min contact time, and at room temperature. The adsorption data exhibited an excellent fit with the Langmuir isotherm model with a maximum adsorption of 68.79 mg g^{-1}. Kinetic studies revealed the adsorption process conformed to a pseudo-second-order model. The nanocomposite fibers demonstrated good reusability over 5 adsorption–desorption cycles. The SLS-PCL/BT nanofiber membrane displayed antibacterial activity against various strains of pathogenic bacteria (*S. aureus*, *B. subtilis*, *E. coli*, and *Salmonella*) with an inhibition zone of 16.56, 19, 25, and 25 mm, respectively. This study demonstrates that SLS-PCL/BT nanofibers are highly effective, reusable adsorbents for removal of MB from aqueous solutions. Moreover, it has antibacterial properties against some bacterial strains.

1. Introduction

Water scarcity, exacerbated by industrial pollution, poses critical challenges to public health and environmental sustainability.[1] Organic dyes, extensively used across different industries such as textiles, paper manufacturing, pharmaceuticals, and cosmetics, represent a considerable threat to ecosystems and human health owing to their persistence, toxicity, and potential carcinogenic properties.[2,3] These pollutants not only contaminate water bodies but also prevent the penetration of sunlight, disrupting aquatic ecosystems and their biological processes. To address this pressing issue, various water treatment methods have been developed, broadly categorized into physical, chemical, and biological approaches.[4,5] Among these, adsorption and membrane technologies have emerged as particularly promising solutions due to their cost-effectiveness, operational simplicity, and reusability.[6–8]

Electrospinning yields nanofiber membranes with high surface area and porosity, ideal for adsorption applications.[9] Electrospinning produces membranes composed of interwoven nanofibers with diameters in the nanometer range, creating structures with exceptional surface area and porosity. These characteristics make them highly effective for adsorption applications, surpassing traditional membrane production methods. The process is influenced by various parameters including solution properties, processing variables, and environmental factors, all of which contribute to the final fiber morphology.[10] Both natural and synthetic polymers can be used in nanofiber synthesis, with synthetic options like polycaprolactone (PCL), polylactide (PLA), polyethersulfone (PES), and polyvinylidene fluoride (PVDF) being favored for their cost-effectiveness and superior mechanical properties.[11] The resulting nanofibers possess several advantageous characteristics, including high surface area-to-volume ratios, adaptable surface modification, reduced density, and excellent pore interconnectivity. These properties can be further enhanced through the incorporation of specific functionalities, such as nanoparticles or surfactants, improving their effectiveness in contaminant removal processes.[12,13]

The versatility of nanofiber-based applications extends beyond water treatment to numerous fields, including tissue engineering, sensors, drug delivery systems, protective clothing, and energy storage.[14] In environmental applications, particularly water treatment, nanofibers demonstrate exceptional

[a]Department of Chemistry, Faculty of Science, Mansoura University, 35516, Mansoura, Egypt

[b]Faculty of Engineering, Mansoura National University, Mansoura, Egypt

[c]Spectroscopy Department, Physics Research Institute, National Research Centre, 33 ElBehouth St., Dokki, 12311, Giza, Egypt

[d]Clinical Chemistry Laboratory, Urology and Nephrology Center, Mansoura University, Mansoura 35516, Egypt. E-mail: w.mortada@mans.edu.eg; Tel: +201022772144

capability in removing various contaminants including heavy metals, persistent organic pollutants, and oily substances.[15] Their effectiveness in both fixed-bed columns and membrane reactors adds to their practical utility. Current research focuses on exploring these applications, particularly in the context of wastewater treatment, where the removal of dyes like methylene blue presents a significant challenge. The continued development and optimization of nanofiber technology promises to play a crucial role in addressing global water pollution challenges while offering sustainable solutions for various industrial applications. This technology's ability to combine high performance with practical applicability makes it a particularly valuable tool in the ongoing effort to protect and preserve water resources for future generations.[16,17]

Nanofibers have become significant as antibacterial surfaces, especially in wound care and medical device coatings, owing to their extensive surface area, porosity, and capacity to integrate antimicrobial chemicals. A study produced electrospun nanofibers synthesized from bacterial cellulose, silver nanoparticles, and Clavanin A, exhibiting substantial suppression of both Gram-positive and Gram-negative microbes, such as *Pseudomonas aeruginosa*. Another method entails the integration of natural extracts; poly (lactic-*co*-glycolic acid) nanofibers infused with aloe vera extract shown antibacterial efficacy against *Staphylococcus aureus* and *Staphylococcus epidermidis*, concurrently facilitating expedited wound healing in diabetic mice. These examples demonstrate the adaptability of nanofibers in improving antibacterial characteristics *via* diverse functionalization techniques.[18]

Here, we fabricate a novel mixed-matrix membrane of SLS-PCL/BT nanofibers using an electrospinning technique. The addition of BT and SLS to PCL membrane improves the adsorption properties and wettability. In this work, the proper incorporation of BT/SLS in the polymeric matrix was evaluated by examining the properties of the resultant membrane using SEM, calculating the contact angle, determining the roughness by AFM. All of this is done with the goal of functioning as a continuous flow system, so providing a novel approach to a significant environmental issue. The prepared nanofiber was applied for removal of methylene blue (MB) from water and for antibacterial properties against *S. aureus*, *B. subtilis*, *E. coli*, and *Salmonella*.

2. Materials and method

2.1. Chemicals

Polycaprolactone $(C_6H_{10}O_2)_n$, (PCL, M_W: 80 000 g mol^{-1}), barium titanate (BaTiO$_3$, ≥99.0%), and sodium lauryl sulfate ($C_{12}H_{25}SO_4Na$, SLS, ≥98.5%) were purchased from Sigma-Aldrich (St. Louis, MO, USA). Methylene blue ($C_{16}H_{18}ClN_3S$, MB, 98.0%), dimethyl formamide (C_3H_7NO, DMF, 99.9%) and chloroform (CHCl$_3$, 99.8%) were supplied from Merck (Darmstadt, Germany). A 1000 mg per L stock solution of MB was prepared by dissolving 1.0 g of the dye in 1000 mL of distilled water. Various concentrations of MB were then obtained by appropriate dilution.

2.2. Preparation of polycaprolactone@barium titanate nanofibers

PCL (1.0 g) was dissolved in 10.0 mL of CHCl$_3$: DMF (8 : 2 v/v) mixture under magnetic stirring for 4 h at room temperature. In the subsequent step, different percentages of BT (0, 0.5, 5.0, 10, 15, and 20) w/v% were added to 10 w/v% PCL solution. Each of the PCL/BT solutions was placed in a plastic syringe with a needle of 14.5 mm in diameter. Electrospinning equipment (Nano-01A) was used for the horizontal electrospinning process. The chosen voltage values produce homogeneous fiber electrospun membranes devoid of structural beads. The applied voltage selected, the feed rate of the PCL solution, and the distance between the tip and collector were 20 kV, 0.5 mL h^{-1}, and 15 cm, respectively. The formed membranes were dried under vacuum for 24 h at ambient temperature.

2.3. Fabrication of polycaprolactone@barium titanate nanofibers

The PCL/BT nanofibers obtained were modified by three methods, *i.e.*, plasma treatment (P-PCL/BT), alkaline activation (OH-PCL/BT), and surfactant addition (SLS-PCL/BT), to improve the adsorption properties.

2.3.1. Plasma treated fibers. The PCL/BT nanofibers were modified by air plasma for 10 min using a plasma cleaner – pcd001-Hp (Plasma Etch, Inc., USA). During the plasma process, RF power of 75 W, a chamber pressure of 100 mTorr, and air flow of 10 SCCM were employed.

2.3.2. Activation by NaOH. The Nanofiber (PCL/BT) was immersed in different concentrations (1.0–2.0 mol L^{-1}) of NaOH (Merck, Germany) aqueous medium for different periods (1–8 h) under shaking (250 rpm) at room temperature. The nanofiber was then extracted and washed with distilled water until the pH of the eluent reaches 7.0. After that the activated nanofiber (OH-PCL/BT) was dried under vacuum for overnight at 37 °C.

2.3.3. Surfactant-fabricated nanofibers. SLS-PCL/BT nanonofiber was prepared by dissolving 1 g PLA and 0.25 g BT in 10 mL a mixture of CHCl$_3$–DMF (8 : 2) with stirring at 250 rpm for 4 h at ambient temperature. Then, 0.1 g of SLS was added to the PCL/BT solution under continuous stirring for 1 h to attain a uniform solution. The SLS-PCL/BT solution was loaded in 10 mL a plastic syringe in electrospinning equipment under the same device parameters as mentioned previously in the step of preparing PCL/BT nanofiber.

2.4. Characterization of nanofiber membranes

The surface morphology of the nanofiber membrane was examined with a scanning electron microscope (SEM), (Quanta 250 FEG, FEI, USA). Functional groups and chemical bonds within the nanofiber samples were identified by FT-IR spectra between 4000–500 cm^{-1} using a Nicolet i10 FT-IR spectrometer (Thermofisher Scientific, USA). An atomic force microscope (AFM) (flex AFM3, Switzerland) was utilized to acquire 3d image and determine the roughness of the nanofiber surface, the scan area: 10 × 10 μm^2 and the number of data points: 256 × 256 at

the scan rate: 1 Hz. The AFM operated in tape mode using a nano conductive silicon probe using nanosurf C3000 (version 3.5.0.31) software Magnetic stirrer (VELP, SCIENTIFIC, Italy) was utilized for the stirring of solutions. GALLENKAMP (flask Shaker, five speeds) was used for shaking. Analytical balance (Mettler AJ150, USA) was used to accurately measure the weight of the substance. The solution pH was determined using a pH meter (Jenway 3310, UK).

2.5. Contact angle measurement

The sessile drop technique is used for determining the contact angle on SLS-PCL/BT nanofiber, which involves placing a small drop of liquid (water) by micropipette on a solid surface (SLS-PCL/BT nanofiber).[19] After that a high-resolution camera (Casio high speed camera EX-F1) captured a side view of the droplet, and then the contact angle was estimated by detecting the droplet outline and fits a tangent line at the point where the droplet meets the surface of nanofiber.

2.6. Point of zero charge

The pH drift method was employed to evaluate the point of zero charge (pH_{pzc}) of the adsorbent.[20] A sequence of bottles was prepared containing a mixture of 50.0 mg of SLS-PCL/BT and 20.0 mL of a 0.05 mol per L KCl solution, at initial pH (pH_i) ranged from 2.0 to 12.0 by adding 0.1 mol L^{-1} of NaOH or HCL. The bottles were agitated (150 rpm) at 25 °C for 24 h. The final pH (pH_f) of the supernatant was determined. The shift in pH ($\Delta pH = pH_f - pH_i$) was plotted against pH_i, and the point of intersection of the curve with the x-axis was determined to obtain pH_{pzc}.

2.7. Adsorption study

The purpose of the batch experiment was to improve the adsorption process and examine the effects of different parameters on the adsorption performance, including pH, contact period, adsorbent dose, dye concentration, temperature, and salt. MB dye adsorption experiment was executed under experimental variables were selected as follows: pH (3–12) was controlled with 0.1 mol per L NaOH and 0.1 mol per L HCl solution, contact time (15–240 min), adsorbent dosage (20–100 mg), initial MB dye concentration (20–200 mg L^{-1}), temperature (25–80 °C), and salt (0.2–5.0 w/v%) by shaking in a sequence of bottles containing 20 mL of MB dye solution at 200 rpm. The concentration of the remaining MB in the solution was measured spectrophotometrically at 668 nm. The adsorption capacity (q_e) and percent removal (R) of MB were estimated by using eqn (1) and (2), respectively.

$$q_e (\text{mg g}^{-1}) = \frac{V(C_0 - C_e)}{m} \tag{1}$$

$$R(\%) = \frac{(C_0 - C_e)}{C_0} \times 100 \tag{2}$$

where, C_0 and C_e are the initial and equilibrated concentrations of MB (mg L^{-1}), respectively, V is the initial volume of the solution (in L) and m (g) is the dry mass of the sorbent.

2.8. Desorption study

For desorption study, 60 mg of SLS-PCL/BT nanofiber was soaked in 25 mL of 50 mg L^{-1} of MB solution for 180 min at 250 rpm at room temperature. After that, the sorbent was thoroughly washed with distilled water to get rid of the extra dye. The sorbent was treated with 20 mL of various eluents (0.1 mol per L HCL, 0.1 mol per L NaOH, or ethanol) for 30 min at 250 rpm. Finally, the sorbent was washed again by distilled water, dried, and then exposed to another adsorption–desorption cycle to investigate the reusability of SLS-PCL/BT nanofiber. The % desorption of MB dye was determined as:

$$D \% = \frac{C_d V_d}{(C_0 - C_e)V} \times 100 \tag{3}$$

Here, C_d represents the concentration of MB that has been desorbed, measured in mg L^{-1}; V_d is the volume of the eluent used, in L. C_0 and C_e denote the initial and equilibrium concentrations of MB (mg L^{-1}), respectively, while V refers to the initial volume of the solution, also in L.

2.9. Antibacterial activity

Antibacterial activity of SLS-PCL/BT nanofiber was performed against *Staphylococcus aureus* (*S. aureus*, ATCC6538), *Bacillus subtilis* (*B. subtilis*, DMS 1088), as Gram-positive, and *Escherichia coli* (*E. coli*, ATCC 10536), and *Salmonella typhimurium* (ATCC 25566) as Gram-negative bacteria. These strains were selected to represent both bacterial classes commonly found in water contamination. In brief, the pure cultures of the bacteria were suspended in Mueller–Hinton agar plates, and the concentration of bacterial suspension was modified to 10^6 colony-forming units (CFU) per mL utilizing a spectrophotometer at 600 nm. The sample discs (10 × 10 mm) were positioned on the surface of agar plates that had been inoculated with the test microorganisms. The plates were incubated at 37 °C. Diameters of inhibition zones (mm) around PCL with different concentrations of BT (0, 5.0, 10, and 20) w/v% and SLS-PCL/BT nanofibers were evaluated after 18–24 h for bacteria. Azithromycin (2 mg mL^{-1}) was used as the positive control.

3. Result and discussion

The preliminary investigation indicated that the synthesized PCL nanofiber had poor adsorption efficiency for MB (20%) and no effect against the target bacteria. To enhance the capacity of adsorption and the antibacterial activity of the fibers, PCL was fabricated with BT. However, the improvement was not as expected (the adsorption efficiency did not exceed 52.0% with no antibacterial activity). To further enhance the properties of PCL/BT nanofiber, several methods were used such as plasma treatment, alkaline activation, and surfactant addition to yield different fabricated fibers denoted as P-PCL/BT, OH-PCL/BT, and SLS-PCL/BT, respectively. The adsorption rates significantly increased to 78.86%, 85.5%, and 90.06% for P-PCL/BT, OH-PCL/BT, and SLS-PCL/BT, respectively. Among them, only SLS-PCL/BT exhibited a marked antibacterial activity against

the studied bacteria. Therefore, in this study we focused on the surfactant-based fibers (SLS-PCL/BT).

3.1. Characterization of nanofiber membrane

3.1.1. AFM study. In this investigation, AFM was used to examine the nanofibers' surface morphology. AFM is a dependable method for obtaining a microscopic view of the surface and quantitatively characterizing its roughness. The average surface roughness (S_a) is typically used to assess the surface roughness of samples. As recorded in Table 1, the BT concentration increases, resulting in raised average roughness of nanofiber and SLS-PCL/BT nanofiber was the highest S_a followed by PCL/BT and PCL nanofiber. An increase in surface roughness results in an enhancement of the surface area, wettability, and promoting dye adhesion, and potentially improving the adsorption process.[21] Moreover, the change in the roughness of the nanofiber membranes may also impact the hydrophilic property of the electrospin nanofiber according to Wenzel model (Fig. 1).[22]

3.1.2. SEM investigation. Fig. 2 illustrates the morphology and structural characteristics of the PCL nanofibers and their composite. The PCL nanofiber had a connected network structure and a smooth fiber surface. One possible explanation for the PCL membrane's interconnected network structure is that the solvents employed in the electrospinning process did not evaporate completely.[23] It was observed that when adding different amounts of BT to PCL, there was no observed change in the morphology of the resulted membranes. On the other hand, when the BT concentration increased from 0 to 20 w/v%, the fiber diameter decreased. Reduction-in nanofiber diameter significantly enhance dye removal efficiency due to the increased specific surface area, higher surface density and improved diffusion of dye molecules through the interconnected porous network. SLS-PCL/BT nanofibers exhibited smooth, homogeneous, bead-free morphology with diameters of 350–512 nm Fig. 2. It was noticed that the addition of SLS led to the aggregation of nanofibers, which is expected to enhance their mechanical strength and water stability.

3.1.3. FTIR-ATR analyses. FTIR optical absorption spectral data was employed to identify the functional groups present on the synthesized nanofibers and to approve the successful interaction with Barium Titanate (BT) and Sodium Lauryl Sulfate (SLS). The spectrum of pristine PCL nanofibers shown in Fig. 3 reveals presence of a characteristic bands at
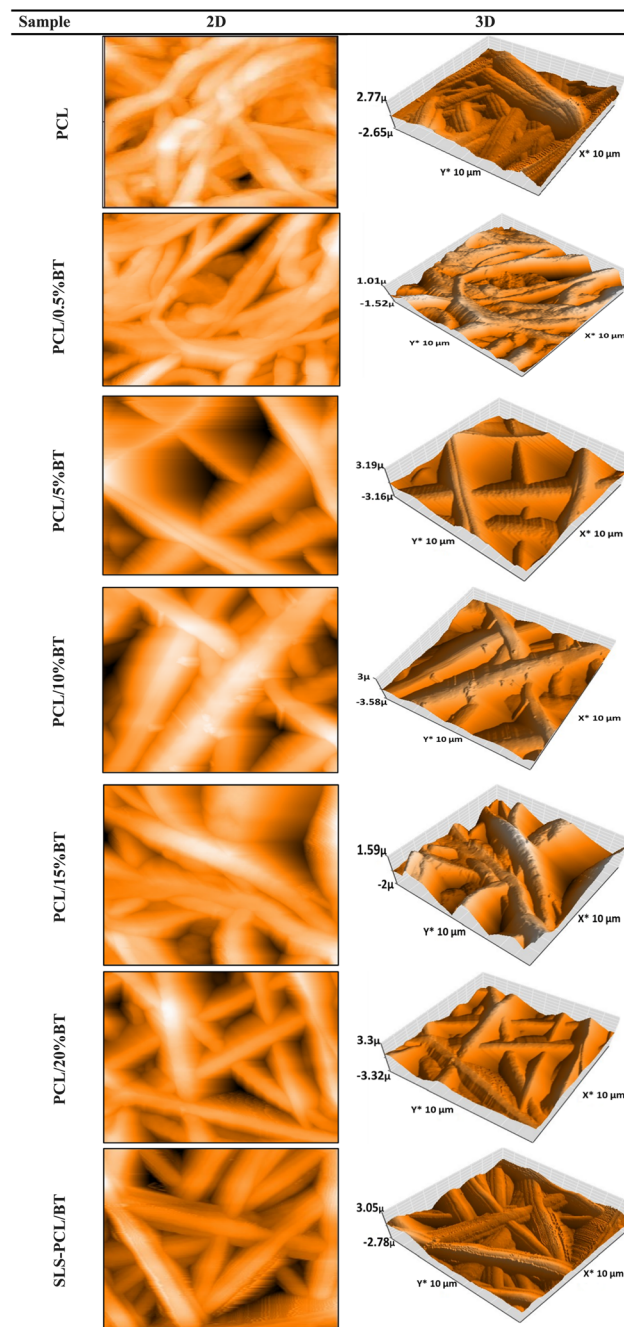
Table 1 Average surface roughness (S_a) of nanofibers

Sample	Value of average roughness S_a (nm)
PCL	223.02
PCL/0.5%BT	275.85
PCL/5.0%BT	344.73
PCL/10%BT	436.69
PCL/15%BT	508.38
PCL/20%BT	547.55
SLS-PCL/BT	578.57

Fig. 1 AFM images of the prepared nanoomposite fibers.

approximately 2942 and 2864 cm^{-1}, corresponding to the asymmetric and symmetric stretching vibrations of CH$_2$ groups, respectively. The strong band at ~1720 cm^{-1} is attributed to the C=O stretching vibration of the ester carbonyl group in PCL. Peaks in the region of 1300–1000 cm^{-1} are associated with C–O and C–C stretching vibrations, while those at 1470 and 1360 cm^{-1} are due to CH$_2$ bending vibrations.[24,25] In other hand PCL/BT spectra shows a a slight but consistent shift or broadening of the carbonyl (C=O) peak at ~1720 cm^{-1} which suggests a potential electrostatic interaction or weak coordination between the ester oxygen of PCL and the surface ions of the
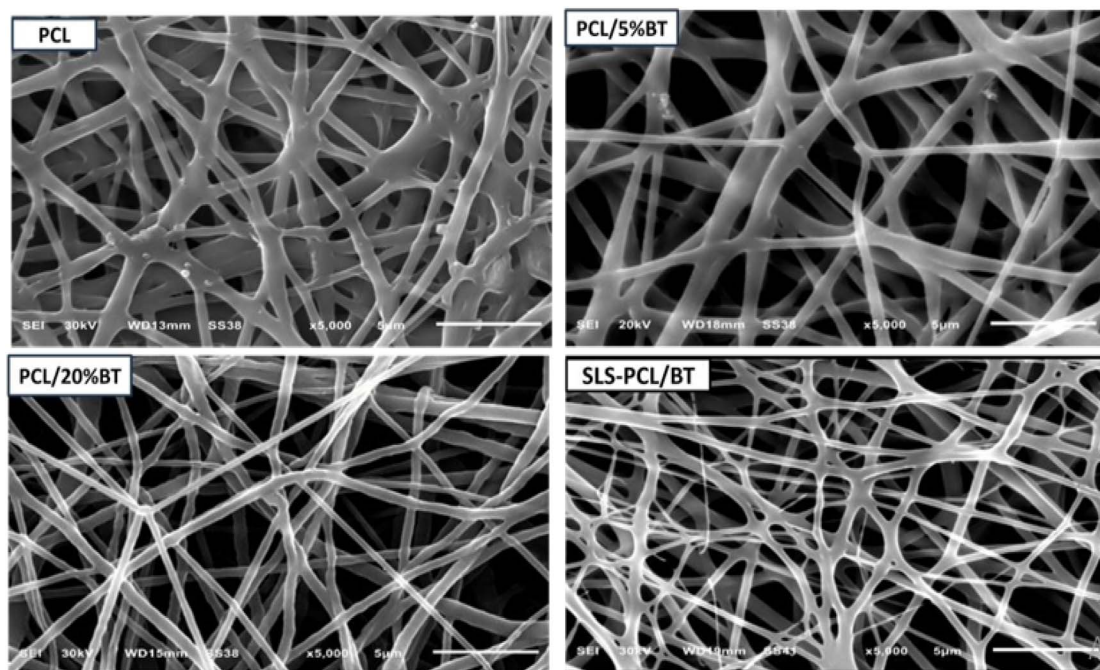
Fig. 2 Morphology and structural characteristics of nanofibers according to SEM images.

BT nanoparticles, confirming the successful integration of BT into the polymer matrix. Moreover, the spectrum of SLS-PCL/BT reveals the most significant changes, directly supporting the proposed adsorption mechanism. New, distinct peaks emerge at approximately 1222 cm^{-1} and 1085 cm^{-1}, which are characteristic of the asymmetric and symmetric stretching vibrations of the sulfonate group (S=O) in SLS.[26] The appearance of these peaks is a clear fingerprint of the anionic surfactant on the fiber surface. The main FTIR signals and their interpretation are listed in Table 2.

3.1.4. Contact angle. The wettability of membranes is a key factor in assessing their appropriateness for various water treatment processes. PCL nanofiber has a contact angle of 115°

indicating that neat PCL possesses hydrophobic characteristic, as shown in Fig. 4. The PCL chains' hydrophobic characteristic is primarily caused by the presence of CH$_2$ groups in their backbone. The hydrophobic characteristic of neat PCL may restrict its wide utilization. Therefore, adding some additive to PCL may be a practical method of increasing the hydrophilicity of PCL. It can be observed that the contact angle dramatically reduces with additional BT and SLS in the nanofiber structure from 115° to 0° (complete wetting). Therefore, adding nanoparticles (BT) and surfactant agents (SLS) to PCL may be a workable strategy to increase PCL's hydrophilicity, as illustrated in Fig. 4. As a result, it is possible to change the surface topography of the membrane and raise the surface roughness and this agreement with the result of AFM analysis, which is necessary to cause the surface to become highly wettable. Similar result was mentioned in ref. 27.
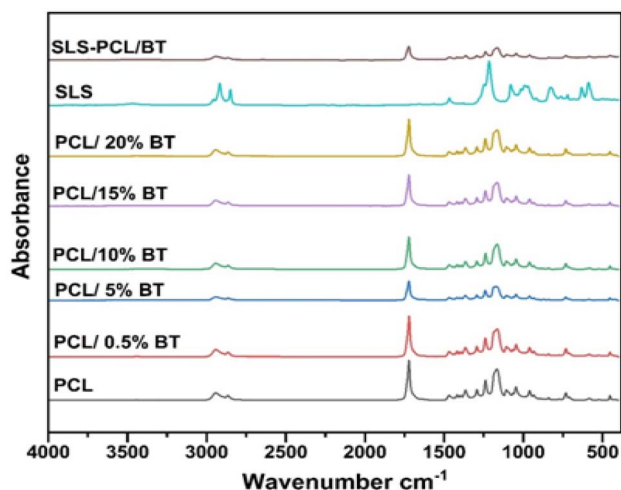
3.2. Impact of BT and SLS incorporation on the fundamental characteristics of fibers

Incorporating varying percentages of BT into the polymer solution for nanocomposite fiber fabrication resulted in notable alterations in the fiber properties. BT is deposited onto the granules' highly porous surface, significantly enhancing the available surface area and thereby promoting effective dye adsorption. As displayed in Fig. 5, by rising the percentage of BT, the adsorption rate of the dye improves. In addition to, the modified PCL/BT nanofiber by anionic surfactants such as SLS demonstrated a pronounced adsorption capacity toward MB dye molecules, where the removal efficiency of MB increased by about 37.9%, owing to the ionic coupling between the cationic MB particles and the anionic surfactant. Adsorption is

Fig. 3 FTIR spectra of the fabricated fibers.

Table 2 FTIR spectral data analysis of PCL nanofibers and composites

Wavenumber (cm^{-1})	Assignment and observations
Pristine PCL	
2942, 2864	Asymmetric & symmetric CH$_2$ stretching
	Characteristic bands of the polymer backbone
~1720	C=O stretching (ester carbonyl)
	Strong band confirming the PCL ester group
1470, 1360	CH$_2$ bending vibrations
	Further confirmation of hydrocarbon chains in PCL
1300–1000	C–O and C–C stretching vibrations
	Expected vibrations for the polymer structure
PCL/BT composite	
~1720	C=O stretching (ester carbonyl), slight shift/broadening of the peak. Suggests electrostatic interaction or weak coordination between PCL's ester oxygen and BT nanoparticles, confirming successful integration
SLS-PCL/BT composite	
~1720	C=O stretching (ester carbonyl) (implied presence, used as reference for other changes)
1222, 1085	Asymmetric & symmetric S=O stretching (sulfonate group)
	New, distinct peaks. A clear fingerprint confirming the successful adsorption of sodium lauryl sulfate (SLS) onto the fiber surface

significantly impacted by the chemical nature of the surfactant's functional groups. It is simple to dissociate and exchange MB ions with the cations linked to the strong acid conjugate base of SLS in an aqueous solution, including sodium ions (R-SO$_3^-$-Na$^+$) and protons (R-SO$_3^-$-H$^+$).[28] It was observed that the SLS-PCL/BT nanofiber demonstrated a strong MB removal, because there are active hydrophilic groups of SLS. MB removal efficiency reached 90.1% at 50 mg per L initial concentration.

3.3. Adsorption study

3.3.1. Effect of pH. The value of pH$_{PZC}$ of SLS-PCL/BT nanofiber was 8.1 as shown in Fig. 6B, indicating that the surface of the nanofiber is positively charged at pH values below 8.1 and negatively charged above this value. pH influences the adsorbent's surface charge, functional group ionization, and dye chemistry.[28] The adoption of MB by SLS-PCL/BT nanofiber was examined in the pH range (2–12). Fig. 6A shows that at low pH, the uptake of MB is poor but it progressively increases with the pH, reaching optimum level at pH 12. When the pH is low, the high concentration of hydrogen ions (H$^+$) encourages protonating the functional groups of SLS-PCL/BT membrane, and this competes with MB dye for active sites due to the high total positive charge. At elevated pH, the surface of the SLS-PCL/BT nanofiber becomes more negatively charged, improving
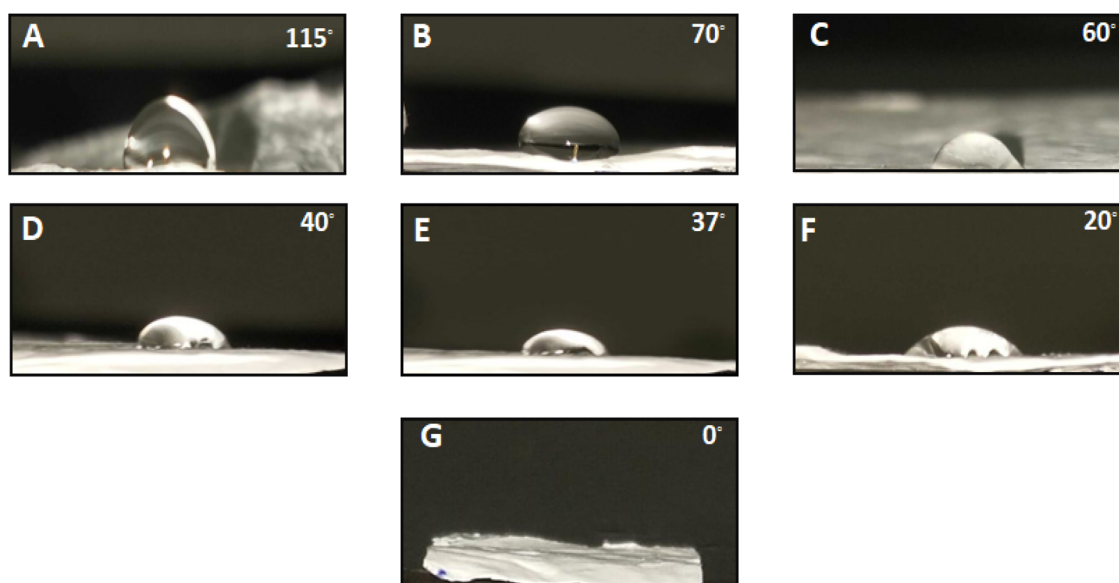

Fig. 4 Contact angles values of the nanofibers membranes of (A) PCL, (B) PCL/BT 0.5%, (C) PCL/BT 5%, (D) PCL/BT 10%, (E) PCL/BT 15%, (F) PCL/BT 20%, and (G) SLS-PCL/BT.
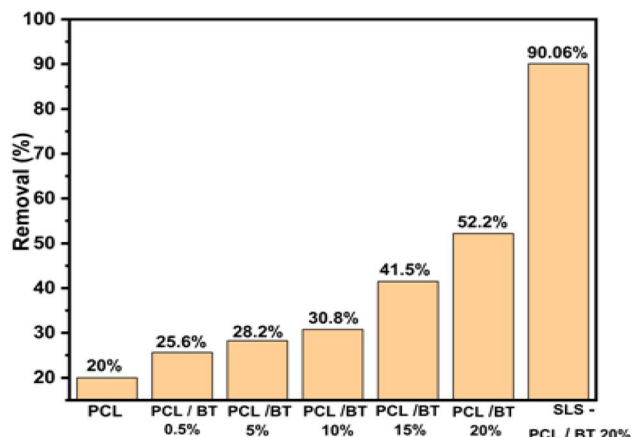
Fig. 5 Influence of BT content (0, 0.5, 5, 10, 15 and 20 w/v%) and SLS added into PCL nanofiber on the methylene blue adsorption.

Fig. 7 Adsorption of MB dye onto SLS-PCL/BT nanofiber: impact of contact time (dye concentration 50 mg L^{-1}, pH = 12, adsorbent dosage 60 mg, temperature 25 °C).

adsorption of the cationic particles. Additionally, as pH increased, the fibers' electronegativity also increased which facilitates the electrostatic interaction between the dye and the SLS-PCL/BT nanofiber. A similar result has been reported by previous authors for other sorbents.[5,29] Based on these findings, pH 12 was evaluated as the suitable pH for eliminating MB.

3.3.2. Impact of contact time. To evaluate the effect of contact time (ranging from 5 to 180 min) on the removal of MB using SLS-PCL/BT nanofibers, experiments were conducted under the following conditions: initial dye concentration of 50 mg L^{-1}, pH 12, adsorbent dosage of 60 mg, and temperature of 25 °C. The removal efficiency increased markedly during the first 60 min, attributed to the plentiful active sites available on the surface of the nanofibers, as shown in Fig. 7. The system reached the equilibrium in around 180 min. Beyond this point, the diffusion of MB dye into the internal pores slowed down considerably. This slower phase was likely due to the saturation of external pores and the full occupation of functional groups
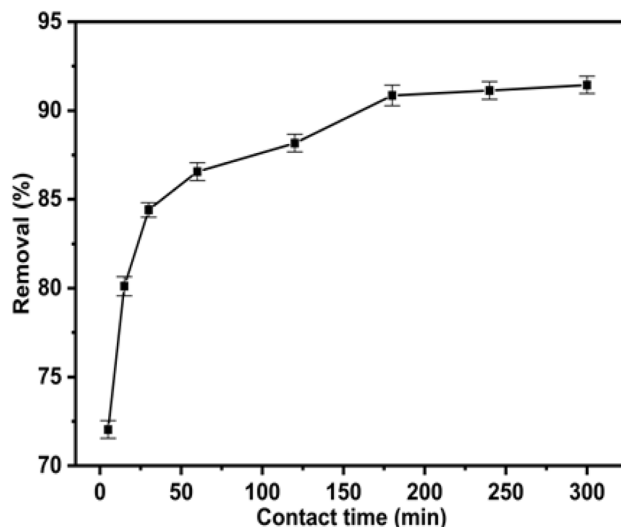
on the adsorbent. Based on these observations, a contact time of 180 min was identified as optimal for maximum removal of MB dye.

3.3.3. Effect of adsorbent dosage. The effect of SLS-PCL/BT nanofiber dosage from 3 to 80 mg on the removal of 50 mg L^{-1} of MB was examined as shown in Fig. 8. It was observed that as the amount of SLS-PCL/BT nanofiber raised from 3 to 60 mg, the removal percentage of MB dye enhanced from 38.5% to 92.7% because there are more adsorbent pores and adsorption sites. At doses higher than 60 mg, there was a slight increase in the percentage of MB adsorption. 60 mg was selected as the best adsorbent dose for the other investigations.

3.3.4. Influence of initial concentration of the adsorbate. Fig. 9 displays the impact of the initial concentration of the dye
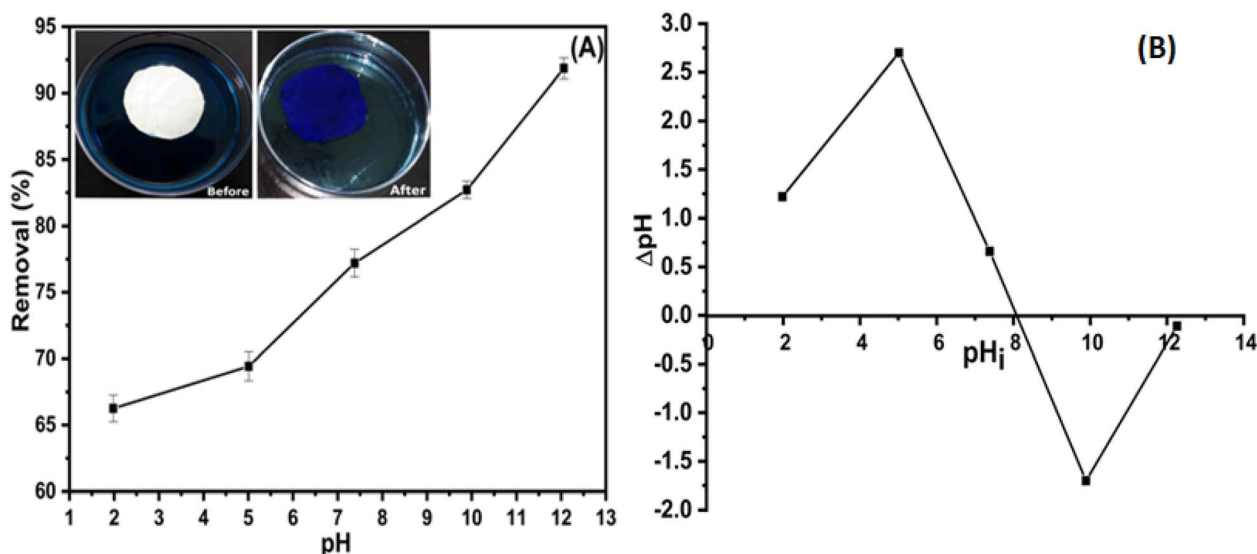

Fig. 6 (A) The impact of pH on the adsorption of MB by SLS-PCL/BT (concentration of the dye 50 mg L^{-1}, adsorbent dosage 60 mg, contact period 120 min, temperature 25 °C) and (B) pH$_{pzc}$ of SLS-PCL/BT nanofiber.
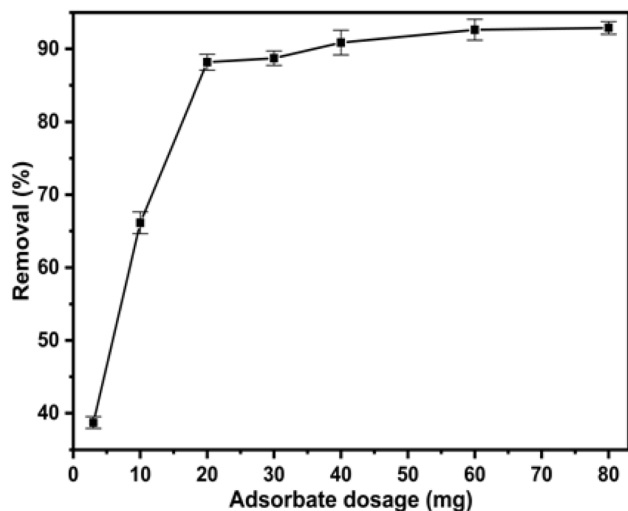
Fig. 8 Impact of varying adsorbent dosage on the adsorptive performance of SLS-PCL/BT nanofibers for MB eliminate (dye concentration 50 mg L^{-1}, contact time 180 min, pH = 12, temperature 25 °C).
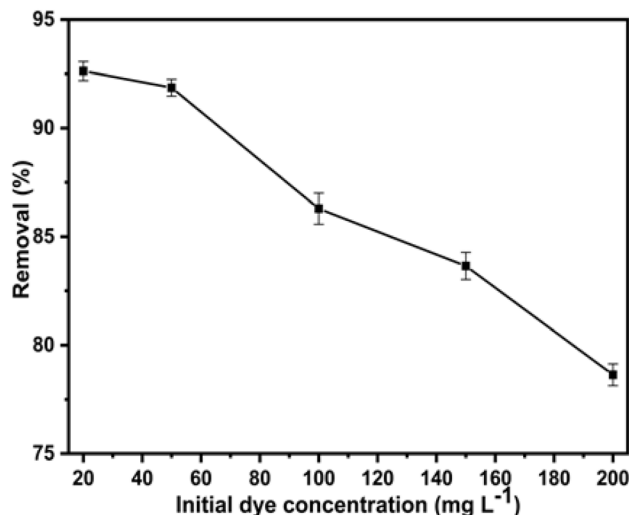

Fig. 9 Impact of concentration of the dye on the adsorption of MB dye onto SLS-PCL/BT nanofiber (adsorbent dosage 60 mg, contact time 120 min, pH = 12, temperature 25 °C).

(20–200 mg L^{-1}) on the adsorption of MB dye. The results showed that the removal percentage was found to drop from 92.6 to 78.6 as the concentration raise from 20 to 200 mg L^{-1}. The maximum adsorption was observed within the concentration range of (20–50 mg L^{-1}) due to the tendency of MB dye tends to create larger molecular aggregates at higher concentrations, that unable enter the interior pores of the adsorbent. Moreover, at higher concentration of MB dye, saturation of the active sites on the SLS-PCL/B nanofiber, leading to a noticeable reduction in removal efficiency as illustrated in Fig. 9. Similar result was recorded in another study.[28]

3.3.5. Influence of temperature and adsorption thermodynamics. The impact of temperature on MB adsorption onto SLS-PCL/BT nanofiber was studied at various temperatures (25, 40, 60 and 80 °C), and the results obtained are illustrated in Fig. 10A. It was observed that the SLS-PCL/BT nanofiber's ability to remove MB decreases with rising temperature. This behavior suggests that the adsorption process proceeds *via* an exothermic. A possible explanation for this result is the reduction in the adsorptive forces holding the MB dye molecules to the SLS-PCL/BT nanofiber's active sites.[30] The adsorption thermodynamic factors including change in free energy ($\Delta G°$), change in enthalpy ($\Delta H°$), and change in entropy ($\Delta S°$) have been employed to understand the variation in the extent of MB dye adsorption onto SLS-PCL/BT nanofiber with temperature. These parameters were determined based on the equations presented below, and the calculated values are recorded in Table 3.

$$\Delta G° = -RT \ln K_L \tag{4}$$

$$\ln K_L = \frac{\Delta S°}{R} - \frac{\Delta H°}{RT} \tag{5}$$

$$K_L = \frac{q_e}{C_e} \tag{6}$$

where K_L (L mol^{-1}) is adsorption equilibrium constant, q_e is equilibrium adsorption capacity, C_e is equilibrium concentration (mg L^{-1}), R is the gas constant (8.314 J mol^{-1} K^{-1}), and T is the temperature (K). According to the results, the desorption of the adsorbed MB dye molecules from SLS-PCL/BT nanofiber is preferred at high temperatures since the K_L values reduced as the temperature rose, shifting the equilibrium to the left.[31] The slope and intercept of the ln K_L *versus* $1/T$ plot as illustrated in Fig. 10B were employed to determine the values of $\Delta H°$ and $\Delta S°$ and these parameters' values are recorded in Table 3. The results displayed that the negative signs of $\Delta H°$ and $\Delta S°$ were indicative of the exothermic nature of MB dye adsorption onto SLS-PCL/BT nanofiber adsorbent and reduced in randomness at the solid–liquid interface during the adsorption of the MB dye on SLS-PCL/BT nanofiber.[32] As well, the negative values of $\Delta G°$ illustrate the adsorption of MB is spontaneous. When the $\Delta H° < 20$ kJ mol^{-1} show that the adsorption process involves physical adsorption; however, a value between 40–200 kJ mol^{-1} proposed a chemical adsorption,[28] suggesting that the adsorption mechanism involves chemical interactions rather than purely physical adsorption. This chemical adsorption may be attributed to electrostatic attraction and possible hydrogen bonding between the negatively charged –SO$_4^-$ groups of SLS and the cationic MB molecules.

3.3.6. Influence of salt. The influence of concentration of the salt (KCl) on the eliminate of MB was studied using a constant adsorbent dose of 60 mg, at various KCl concentrations of 0.2, 0.4, 0.6, 1.0, 3.0, and 5.0 w/v%. The results revealed that the adsorption efficiency of MB dye onto the SLS-PCL/BT nanofiber gradually decreased as the amount of KCl dosage increased, as shown in Fig. 11. The observed result could be explained by the shielding effect caused by the elevated concentration of inorganic salts, which reduces the abundance
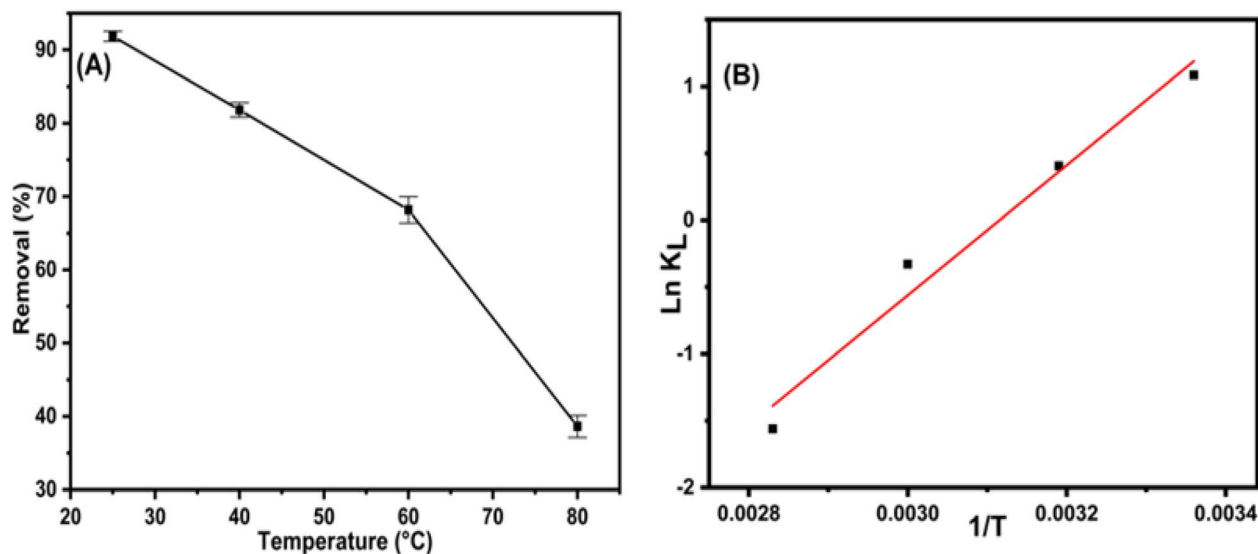
Fig. 10 (A) Impact of temperature on the eliminate of MB by SLS-PCL/BT nanofiber (concentration of the dye 50 mg L^{-1}, adsorbent dosage 60 mg, contact time 180 min, pH = 12), and (B) plot of ln K vs. 1/T for thermodynamic parameters determination.

Table 3 Evaluation of thermodynamic parameters associated with the adsorption of MB onto SLS-PCL/BT nanofiber

Temperature (K)	298	313	333	353
ΔG° (kJ mol^{-1})	−2.69	−1.05	0.90	4.58
K_L	2.96	1.50	0.72	0.21
ΔH° (kJ mol^{-1})	−40.42	—	—	—
ΔS° (J K^{-1} mol^{-1})	−125.96	—	—	—

Table 4 Isotherm model parameters for the adsorption of MB dye onto SLS-PCL/BT nanofiber at 25 °C

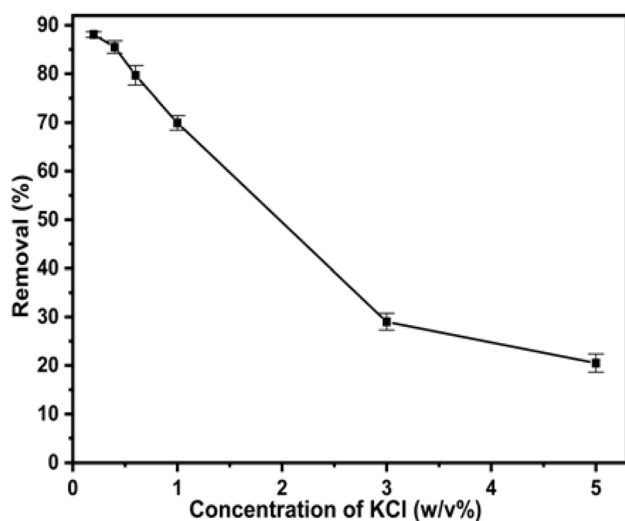| Adsorption isotherm	Parameter	Value
Langmuir	Q_m (mg g^{-1})	68.790
	K_L (L mg^{-1})	0.066
	R^2	0.997
Freundlich	n	1.520
	K_f (mg g^{-1})	4.900
	R^2	0.977
Temkin	B (J mol^{-1})	11.26
	A (L g^{-1})	1.430
	R^2	0.919

Fig. 11 Effect of salt concentration on the removal of MB by SLS-PCL/BT nanofiber (concentration of the dye 50 mg L^{-1}, adsorbent dosage 60 mg, contact period 180 min, pH = 12, temperature 25 °C).

of charged active sites on the adsorbent and consequently inhibits electrostatic interactions with the adsorbat.[33]

3.3.7. Isotherm study. MB dye adsorption onto SLS-PCL/BT nanofiber adsorbent with different initial concentrations (20–

200 mg L^{-1}) was investigated with the remaining other factors constants (pH = 12; dose 60 mg; time 180 min). In the literature, there are several models that examine the adsorption process. In the current study, Freundlich, Langmuir and Temkin models were employed to investigate the adsorption experimental data.[33,34] Table 4 lists the adsorption experimental data isotherm modeling.

The Langmuir model proposes monolayer adsorption, where all sites on the adsorbent are uniform and possess identical capacities.[28,35] The Langmuir's equation is explained as follows:

$$\frac{C_e}{q_e} = \frac{1}{K_L \cdot q_{max}} + \frac{C_e}{q_{max}} \qquad (7)$$

where C_e is MB equilibrium concentration (mg L^{-1}), q_e is the equilibrium adsorption capacity at distinct concentration of the MB (mg g^{-1}), K_L (L mg^{-1}) is Langmuir constant and q_m (mg g^{-1}) is the adsorption capacity of fabricated adsorbent. Adsorption is considered to be a multilayer process that occurs on
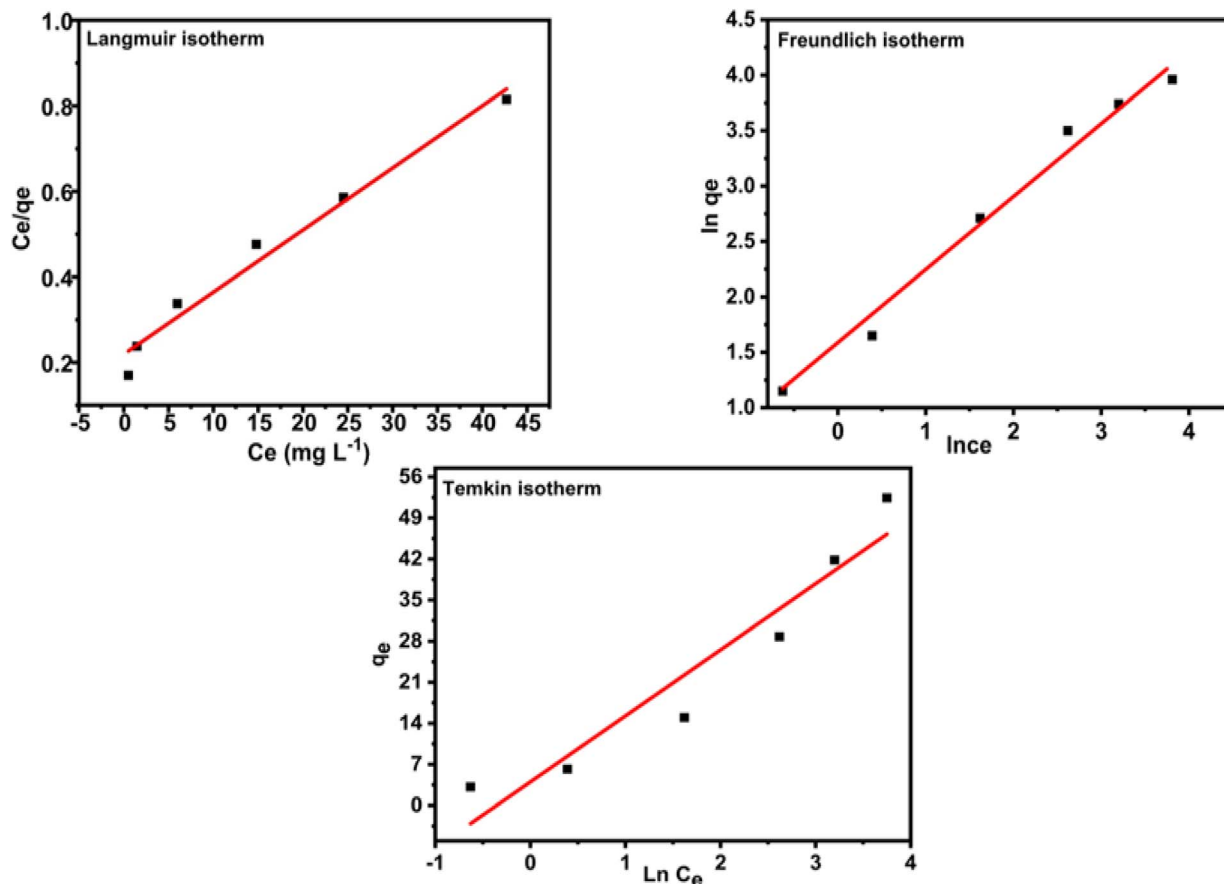
Fig. 12 Linear fitting curve of various isotherm models for the adsorption of MB by SLS-PCL/BT nanofiber.

Table 5 Kinetic models and their factors for the adsorption of MB on SLS-PCL/BT nanofiber

Kinetic adsorption	Parameter	Value
Pseudo-first order (PFO)	Q_e (mg g^{-1})	7.2300
	K_1 (min)	0.0013
	R^2	0.9700
Pseudo-second order (PSO)	Q_e (mg g^{-1})	9.2000
	K_2 (g mg^{-1} min^{-1})	0.0400
	R^2	0.9990

heterogeneous surface, per Freundlich's model. The Freundlich isotherm linear equation is illustrated in eqn (8):

$$\ln q_e = \ln K_f + \left(\frac{1}{n}\right)\ln C_e \qquad (8)$$

where K_F (mg g^{-1}) is the Freundlich constant; $(1/n)$ is the adsorption intensity. The Temkin model views the adsorbent-contaminant interaction as a chemical adsorption process. The Temkin isotherm equation is illustrated in eqn (9) and (10):

$$Q_e = \frac{RT}{b}\ln A + \frac{RT}{b}\ln C_e \qquad (9)$$

$$B = \frac{RT}{b} \qquad (10)$$

where b (mg L^{-1}) is the Temkin isotherm constant, A (L g^{-1}) is the Temkin isotherm equilibrium binding constant, and B is the constant correlated to the heat of adsorption (J mol^{-1}). Nonlinear curves of isotherms models are illustrated in Fig. 12. Based on the obtained results which were recorded in Table 4, the criteria for selecting the best isotherm model were based on the determination coefficient (R^2) obtained from the nonlinear plots. The Langmuir model is the high correlation coefficient (R^2) of nonlinear isotherm models indicating a superior fit to the experimental data than that's Freundlich and Temkin model. These results indicated that the adsorption of MB on SLS-PCL/BT nanofiber adsorbent was a monolayer adsorption process and the adsorption sites of the adsorbent for MB were uniformly distributed. The maximum adsorption MB on SLS-PCL/BT nanofiber adsorbent was 68.79 mg g^{-1} at room temperature. The homogenous adsorption sites for SLS-PCL/BT nanofiber were produced by the uniform covering of the nanofiber's surface by surfactant molecules. Therefore, it can be assumed that physical and chemical monolayer adsorption was the mechanism of the adsorption of MB by SLS-PCL/BT nanofiber.

3.3.8. Adsorption kinetic. To Study the mechanism and rate of MB adsorbed onto SLS-PCL/BT nanofiber at equilibrium and at time t (min), the kinetic experimental data was analyzed
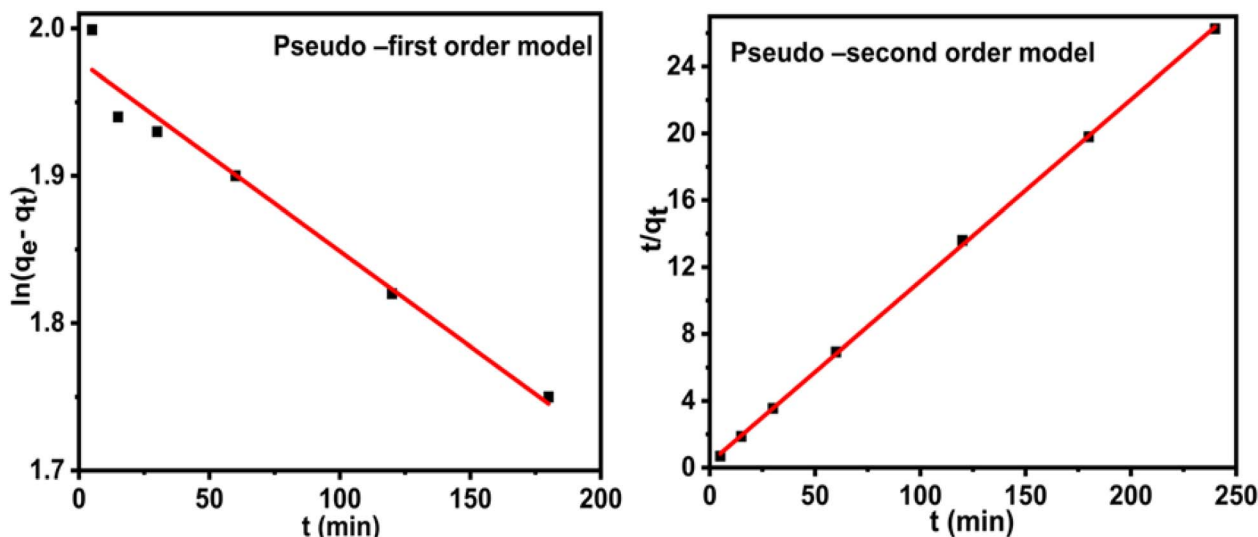
Fig. 13 Nonlinear kinetic adsorption models of MB dye adsorption by SLS–PCL/BT nanofiber.

by models of pseudo-first order (PFO-eqn (11)) and pseudo-second order (PSO-eqn (12)).[36]

$$\ln(q_e - q_t) = \ln(q_e) - k_1 t \tag{11}$$

$$\frac{t}{q_t} = \frac{1}{K_2\, q_e^2} + \frac{t}{q_e} \tag{12}$$

where q_t and q_e (mg g^{-1}) are the adsorbed dose of MB at time t (min) and at equilibration, respectively, and K_1 (min^{-1}) and K_2 (g mg^{-1} min^{-1}) are the rate constant for pseudo-first order and pseudo-second order, respectively. The experimental data and the curve-fitting results of PFO and PSO are illustrated in Table 5 and Fig. 13. The pseudo-second order exhibited a higher correlation coefficient (R^2) compared to the pseudo-first order, indicating that MB adsorption onto the adsorbent surface follows the pseudo-second-order model. The result suggests the

existence of strong binding forces between the adsorbent and the adsorbate, attributed to the complexation of methylene blue (MB) with functional groups on the adsorbent surface. Furthermore, according to the pseudo second-order model, chemisorption is the adsorption process' rate-controlling step.

3.3.9. Desorption and regeneration study. The feasibility of reusing the nanofiber membrane is a significant component in investing it for financial and environmental reasons. Therefore, different eluents (ethanol, HCl, NaOH, and distilled water) were used to determine the ability to remove MB from the surface of SLS–PCL/BT nanofiber. As illustrated in Fig. 14A, the % desorption of ethanol > HCl (0.1 mol L^{-1}) > NaOH (0.1 mol L^{-1}) > distilled water, so ethanol was chosen as the best solvent for desorbing of the dye to regenerate the fibers. It can be observed that the adsorption performance of the nanofiber membrane
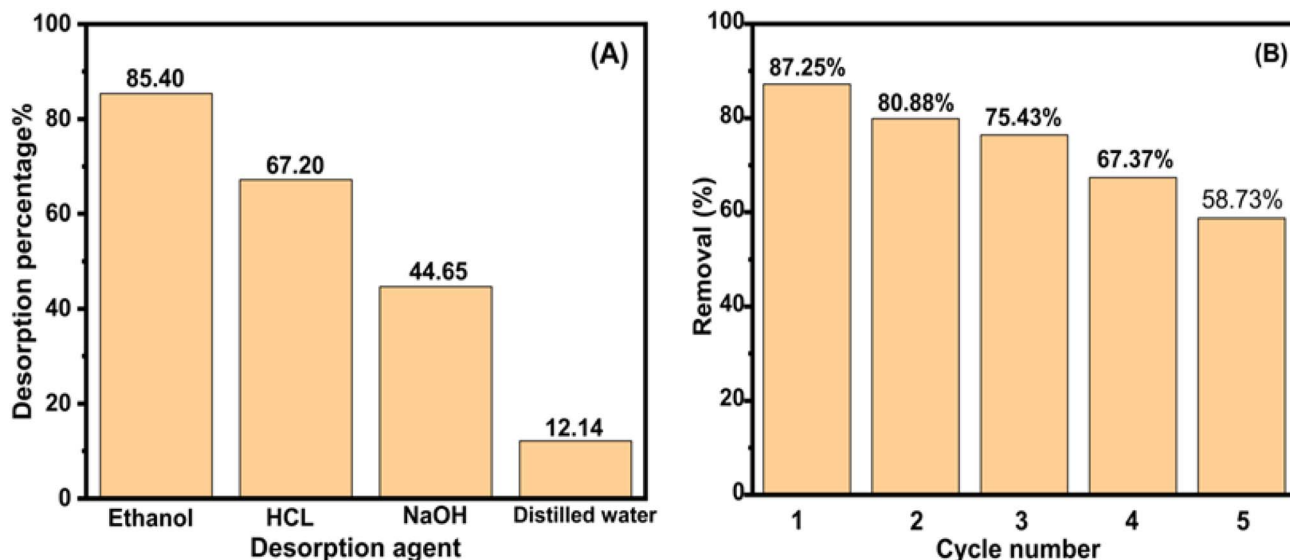

Fig. 14 (A) Desorption and (B) regeneration study for adsorption of MB onto SLS–PCL/BT nanofiber.
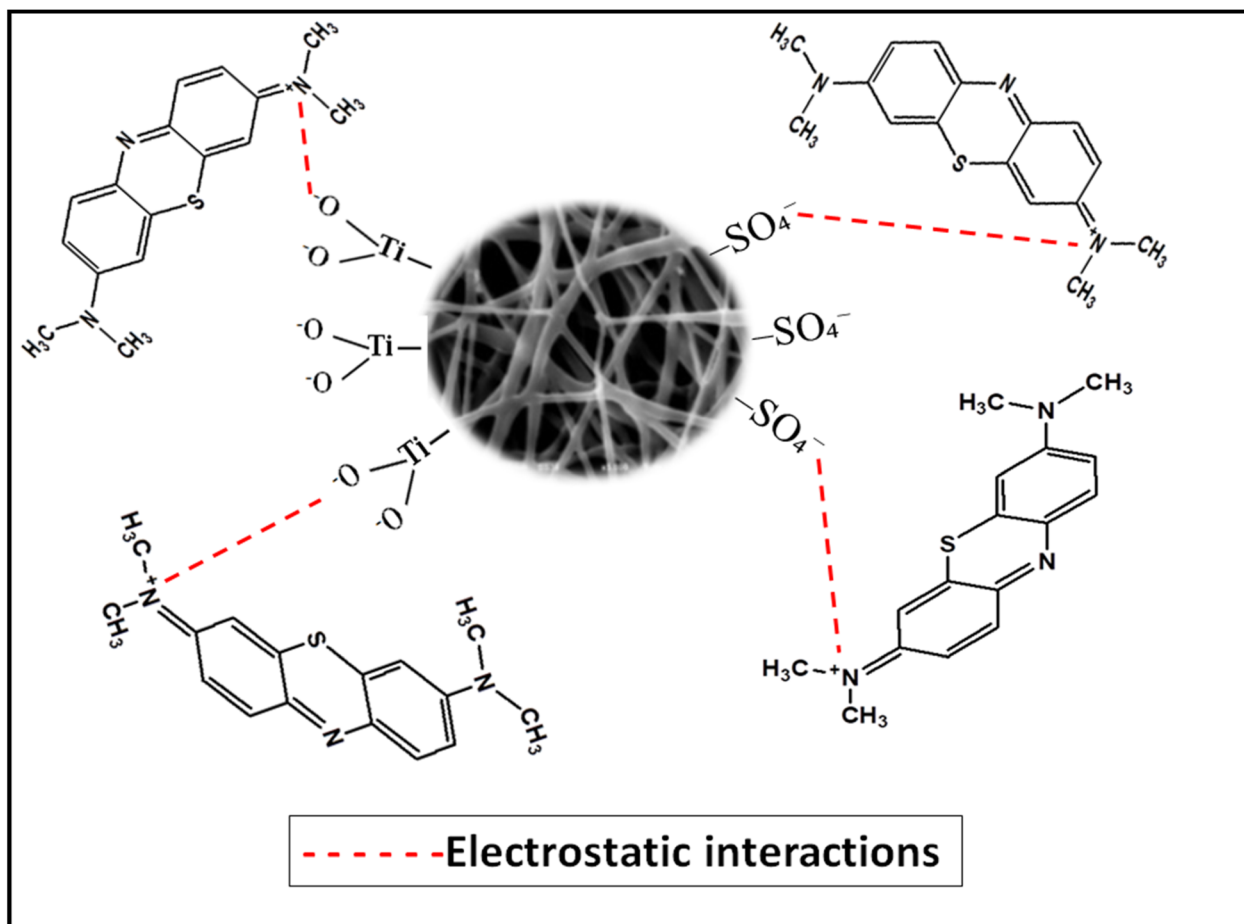
Fig. 15 The suggested adsorption mechanism of MB dye on SLS–PCL/BT nanofiber.

reduced after the fifth cycle as presented in Fig. 14B. The reason for this was that the fiber membrane's texture may turn soft, and repeated adsorption cycles would block the membrane's pores and partially destroy the fiber structure. However, after five adsorption cycles, adsorption efficiency dropped by 33.16% and this indicates the SLS-PCL/BT nanofiber membrane's regeneration capabilities in the MB adsorption process.

3.4. The suggested mechanism for the adsorption process

The integration of SLS and BaTiO$_3$ within PCL nanofibers significantly improves their performance in dye adsorption through a cooperative mechanism. The presence of the anionic surfactant SLS contributes sulfate ($-SO_4^-$) groups to the fiber surface, imparting a strong negative charge and enhancing surface hydrophilicity as illustrated in Fig. 15. These modifications promote the attraction and binding of positively charged dye molecules such as methylene blue (MB) *via* electrostatic interactions and improved liquid penetration.[37] In parallel, the embedded BT nanoparticles introduce polarized and negatively charged regions arising from their dielectric and piezoelectric characteristics, which further intensify the interaction between the fiber surface and the dye species.[38] As a result, the dual incorporation of SLS and BT generates a highly reactive, polar interface that

significantly increases both the adsorption capacity and stability of dye molecules on the PCL nanofiber matrix (Table 6).

3.5. Comparison with different adsorbents

Table 6 shows a comparison between the adsorption capacity of SLS-PCL/BT membrane with that of other adsorbents regarding MB. As indicated the adsorption capacity of the prepared membrane is superior over the other materials.

3.6. Antibacterial activity

In this study, the antibacterial activity of electrospun nanofiber membranes composed of PCL, PCL/BT, and SLS-PCL/BT was evaluated against both Gram-positive (*Staphylococcus aureus* and *Bacillus subtilis*) and Gram-negative (*Escherichia coli* and *Salmonella*) bacteria after 24 h of incubation. The inhibition zones (ZOI, mm) are illustrated in Fig. 16. As shown in Fig. 16A and B, all samples showed negligible inhibition against *S. aureus*, except for the SLS-PCL/BT nanofiber, which exhibited a distinct ZOI of approximately 16.56 mm. In the case of *B. subtilis* (Fig. 16C), the PCL/BT nanofiber demonstrated moderate antibacterial activity about (14.0 mm), whereas the SLS-PCL/BT nanofiber achieved a significantly higher ZOI of about 29.0 mm. For Gram-negative bacteria (Fig. 16D and E), the PCL/BT nanofiber showed no inhibition against *E. coli* or

Table 6 The adsorbent's MB adsorption capacity is compared to that of other adsorbents previously reported

Adsorbents	Q_{max} (mg L^{-1})	Ref.
Acid-factionalized biosorbent derived from coconut shell	50.60	39
Zn-based metal organic framework	26.30	40
Benzimidazole-based covalent organic framework	63.30	41
Uncalcined solution blow spun PAN and PVDF NF membrane	55.91 and 44.06	42
Electrospun crosslinked gelatin/β-cyclodextrin NF membrane	47.40	43
Bacteria-immobilized electrospun nanofiber	48.05	44
Modified PVDF NF membrane incorporated with HAPNP and PVP	10.83	45
Electrospun PAN NF membrane	42.66	46
SLS-PCL/BT NF membrane	68.79	Current study

Salmonella, while SLS-PCL/BT exhibited a pronounced antibacterial effect with inhibition zones of approximately 25 mm for both strains. These findings clearly demonstrate that the incorporation of SLS into the PCL/BT matrix substantially enhances antibacterial performance. The improvement can be attributed to a synergistic effect between SLS and BT. Sodium lauryl sulfate (SLS), an anionic surfactant, interacts with the bacterial cell membrane through electrostatic attraction, disrupting the lipid bilayer, increasing membrane permeability, and causing leakage of intracellular components.[47,48] Meanwhile, barium titanate (BT) nanoparticles contribute by inducing localized surface polarization[49] and generating reactive oxygen species (ROS),[50] which can oxidize cellular constituents and further damage bacterial walls. The combination of these two mechanisms results in stronger antibacterial efficacy. The observed trends are consistent with previous reports,[51,52]
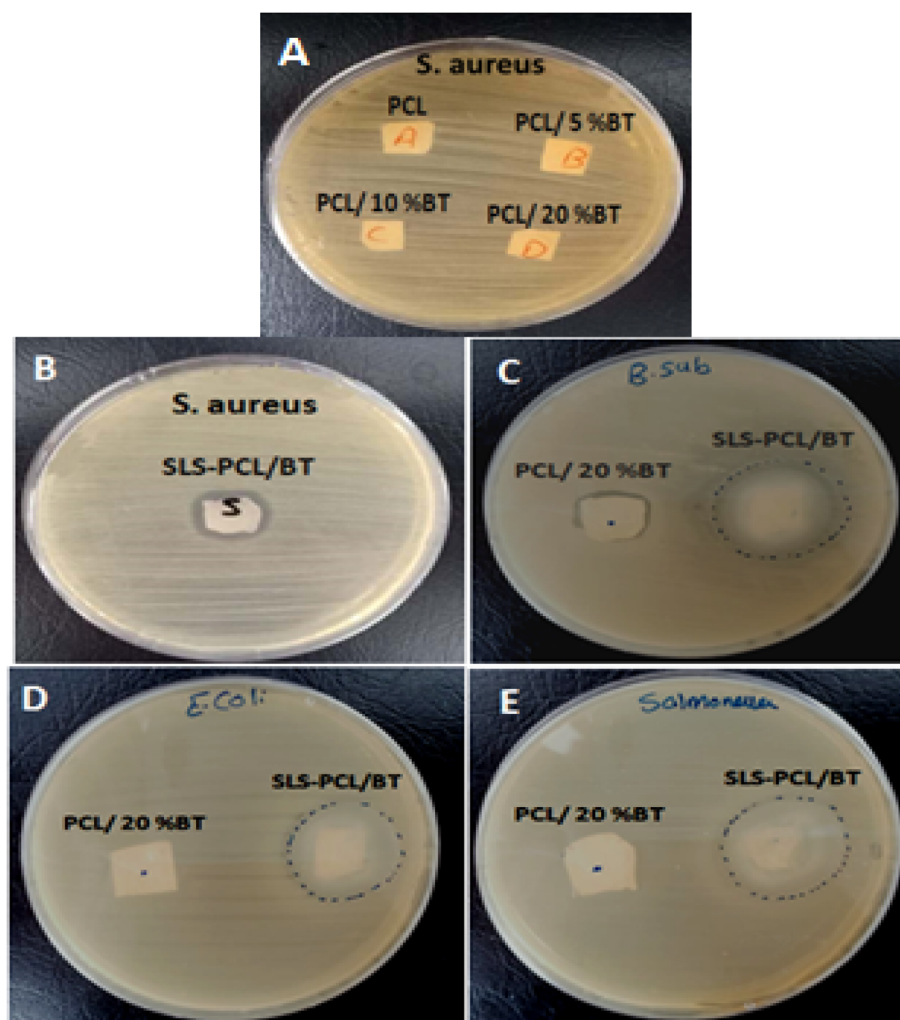

Fig. 16 Antibacterial activities of nanofibers against (A and B) *S. aureus*, (C) *B. subtilis*, (D) *E.coli*, and (E) *Salmonella*.

Table 7 Inhibition zones of electrosun nanofibers against some types of bacteria

Samples name	PCL	PCL/5%BT	PCL/10%BT	PCL/20%BT	SLS-PCL/BT
S. aureus	−ve	−ve	−ve	−ve	16.56 mm
B. subtilis	—	—	—	14.00 mm	29.00 mm
E. coli	—	—	—	−ve	25.00 mm
Salmonella	—	—	—	−ve	25.00 mm

which highlighted that integrating metal oxide nanoparticles with surfactant-modified polymers could yield nanocomposites with markedly improved antimicrobial activity (Table 7).

4. Conclusion

In this work, PCL, PCL/BT, P-PCL/BT, OH-PCL/BT and SLS-PCL/BT nanofibers were fabricated and evaluated for their effectiveness in MB dye and microbial control. The SLS-PCL/BT nanofiber was selected as the best sorbent because it has high efficiency for removing of MB from aqueous media. Functional groups on the surface of SLS-PCL/BT nanofiber, namely ($-SO_3$) and ($-COO-$) play a significant role in the binding of MB dye to the SLS-PCL/BT nanofiber surface, based on the FTIR spectroscopy investigations. And according AFM investigation, SLS can used to increase the hydrophilicity of SLS-PCL/BT nanofiber. Different factors including pH, contact period, dye concentration, adsorbent dose, salt concentration and temperature had a significant impact on SLS-PCL/BT nanofiber's adsorbent performance. pH 12, contact period of 180 min, 60 mg of the adsorbent, an initial concentration of the dye of 50 mg L^{-1} were the ideal working parameters. The Langmuir model exhibited a better fit to the equilibrium adsorption data of MB dye compared to the Freundlich and Temkin models. This suggests monolayer adsorption with a maximum adsorption capacity of 68.79 mg g^{-1} of the SLS-PCL/BT nanofiber at 25 °C and pH 12. The adsorption of MB dye onto SLS-PCL/BT nanofibers was best investigated by the pseudo-second-order (PSO) kinetic model, indicating that the process is governed by chemisorption. Based on thermodynamic results, the adsorption process was exothermic. The regeneration study performed using ethanol demonstrated notable efficiency even after five cycles, with only a 33.16% decrease in removal efficiency. The study demonstrates that SLS-PCL/BT nanofibers exhibit antibacterial activity against *S. aureus*, *B. subtilis*, *E. coli*, and *Salmonella*, with inhibition zones of 16.56, 29, 25, and 25 mm, respectively. This indicates their potential as eco-friendly adsorbents for efficient MB dye removal from aqueous media.

Author contributions

Reem Fathy: data curation, methodology, formal analysis, investigation, writing – original draft. A. M. Abdelghany: data curation, investigation, resources, validation, writing – review & editing. Wael I. Mortada: conceptualization, data curation, resources, supervision, writing – review & editing. E. Abdel-Latif: data curation, investigation, resources, validation, writing – review & editing.

Conflicts of interest

The authors declare that they have no known competing financial interests or personal relationships that could have appeared to influence the work reported in this paper.

Data availability

The data that supports the findings of this study are available from the corresponding author upon reasonable request.

References

1 H. Wei, H. Qiu, J. Liu, W. Li, C. Zhao and H. Xu, Evaluation and source identification of water pollution, *Ecotoxicol. Environ. Saf.*, 2025, **289**, 117499.

2 F. Baahmadi, H. Abbasi-Asl, M. Ghaedi, M. M. Sabzehmeidani and A. Shokrollahi, High-performance cellulose acetate fibers-loaded Alca layered double oxide adsorbents towards efficient elimination of anionic pollutants: Mechanism adsorption and RSM-CCD approach, *Int. J. Biol. Macromol.*, 2025, **284**, 137788.

3 Y. Zhou, J. Lu, Y. Zhou and Y. Liu, Recent advances for dyes removal using novel adsorbents: A review, *Environ. Pollut.*, 2019, **252**, 352–365.

4 J. Lagiewka, K. Witt, M. Gierszewska and I. Zawierucha, Selective removal of organic dyes via polymer inclusion membrane containing a perbenzylated β-cyclodextrin derivative, *J. Water Process Eng.*, 2024, **68**, 106306.

5 W. I. Mortada, M. M. Ghaith, N. E. Khedr, M. I. Ellethy, A. W. Mohsen and A. L. Shafik, Mesoporous magnetic biochar derived from common reed (Phragmites australis) for rapid and efficient removal of methylene blue from aqueous media, *Environ. Sci. Pollut. Res.*, 2024, **31**, 42330–42341.

6 J. Farahbakhsh, M. Najafi, M. Golgoli, A. H. Asif, M. Khiadani, A. Razmjou and M. Zargar, Microplastics and dye removal from textile wastewater using MIL-53 (Fe) metal-organic framework-based ultrafiltration membranes, *Chemosphere*, 2024, **364**, 143170.

7 W. I. Mortada, K. A. Nabieh and A. M. Abdelghany, Efficient and Low-Cost Surfactant-Assisted Solid Phase Extraction Procedure For Removal Of Methylene Blue Using Natural Dolomite, *Water. Air. Soil Pollut.*, 2023, **234**, 1–11.

8 S. Bakhshizadeh, M. Ghaedi, K. Dashtian, M. M. Sabzehmeidani and H. Abbasi-Asl, Molecularly imprinted polymer based on MIL-101 (Cr) MOF incorporated polyvinylidene for selective adsorption and separation dye with improved antifouling properties, *Colloids Surfaces A Physicochem. Eng. Asp.*, 2024, **702**, 134545.

9 Z. Uddin, F. Ahmad, T. Ullan, Y. Nawab, S. Ahmad, F. Azam, A. Rasheed and M. S. Zafar, Recent trends in water purification using electrospun nanofibrous membranes, *Int. J. Environ. Sci. Technol.*, 2022, **19**, 9149–9176.

10 R. Fathy, A. Abdelghany, W. I. Mortada and A. Ehab, Tuning Electrospinning Conditions to Tailor the Diameter and Morphology of Polycaprolactone Nanofibers,, *Egy. J. Chem*, 2025, **68**(5), 263–269.

11 B. M. Thamer, A. Aldalbahi, A. Meera Moydeen, M. Rahaman and M. H. El-Newehy, Modified electrospun polymeric nanofibers and their nanocomposites as nanoadsorbents for toxic dye removal from contaminated waters: A review, *Polymers*, 2021, **23**, 1–37.

12 K. P. Chaithra, A. Varghese, T. P. Vinod and K. R. Sunaja Devi, Multifunctional electrospun membranes incorporated with metal oxide nanoparticles, cellulose acetate, and polyvinylpyrrolidone for wastewater treatment: Oil/water separation, dye adsorption, and dye degradation, *Chem. Eng. J.*, 2024, **499**, 156049.

13 L. Bai, X. Wang, X. Guo, F. Liu, H. Sun, H. Wang and J. Li, Superhydrophobic electrospun carbon nanofiber membrane decorated by surfactant-assisted in-situ growth of ZnO for oil–water separation, *Appl. Surf. Sci.*, 2023, **622**, 156938.

14 A. Nadaf, A. Gupta, N. Hasan, N. Fauziya, S. Ahmad, P. Kesharwani and F. J. Ahmad, Recent update on electrospinning and electrospun nanofibers: current trends and their applications, *RSC Adv.*, 2022, **12**, 23808–23828.

15 S. Wu, W. Shi, K. Li, J. Cai, C. Xu, L. Gao, J. Lu and F. Ding, Chitosan-based hollow nanofiber membranes with polyvinylpyrrolidone and polyvinyl alcohol for efficient removal and filtration of organic dyes and heavy metals, *Int. J. Biol. Macromol.*, 2023, **239**, 124264.

16 T. T. A. Tran, E. Gnoumou, B. L. Liu, P. Srinophakun, C. Y. Chiu, C. Y. Wang, K. H. Chen and Y. K. Chang, Highly efficient capture of Escherichia coli using chitosan-lysozyme modified nanofiber membranes: Potential applications in food packaging and water treatment, *Biochem. Eng. J.*, 2024, **210**, 109411.

17 B. Lomba-Fernández, A. Fdez-Sanromán, M. Pazos, M. A. Sanromán and E. Rosales, Iron metal-organic framework nanofiber membrane for the integration of electro-Fenton and effective continuous treatment of pharmaceuticals in water, *Chemosphere*, 2024, **366**, 143447.

18 R. Abdulhussain, A. Adebisi, B. R. Conway and K. Asare-Addo, Electrospun nanofibers: Exploring process parameters, polymer selection, and recent applications in pharmaceuticals and drug delivery, *J. Drug Deliv. Sci. Technol.*, 2023, **90**, 105156.

19 J. M. Schuster, C. E. Schvezov and M. R. Rosenberger, Influence of Experimental Variables on the Measure of Contact Angle in Metals Using the Sessile Drop Method, *Procedia Mater. Sci.*, 2015, **8**, 742–751.

20 M. Kosmulski, The pH dependent surface charging and points of zero charge. VII. Update, *Adv. Colloid Interface Sci.*, 2018, **251**, 115–138.

21 S. Zhou, X. Bu, X. Wang, C. Ni, G. Ma, Y. Sun, G. Xie, M. Bilal, M. Alheshibri, A. Hassanzadeh and S. C. Chelgani, Effects of surface roughness on the hydrophilic particles-air bubble attachment, *J. Mater. Res. Technol.*, 2022, **18**, 3884–3893.

22 S. Azizian and M. Khosravi, Advanced oil spill decontamination techniques, *Interface Sci. Technol.*, 2019, **30**, 283–332.

23 H. N. Doan, P. P. Vo, A. Baggio, M. Negoro, K. Kinashi, Y. Fuse, W. Sakai and N. Tsutsumi, Environmentally Friendly Chitosan-Modified Polycaprolactone Nanofiber/Nanonet Membrane for Controllable Oil/Water Separation, *ACS Appl. Polym. Mater.*, 2021, **3**, 3891–3901.

24 H. P. Hinestroza, H. Urena-saborio, F. Zurita, A. Alejandra, G. De Le, G. Sundaram and B. Sulbar, Composite Membranes and Their Potential for the Removal of Pollutants from Water, *Molecules*, 2020, **683**, 1–13.

25 C. Qian, Y. Liu, S. Chen, C. Zhang, X. Chen, Y. Liu and P. Liu, Electrospun core–sheath PCL nanofibers loaded with nHA and simvastatin and their potential bone regeneration applications, *Front. Bioeng. Biotechnol.*, 2023, **11**, 1–11.

26 A. Elsayed, M. Al-Remawi, N. Qinna, A. Farouk, K. A. Al-Sou'Od and A. A. Badwan, Chitosan-sodium lauryl sulfate nanoparticles as a carrier system for the in vivo delivery of oral insulin, *AAPS PharmSciTech*, 2011, **12**, 958–964.

27 H. A. Alrafai, Z. Ali Al-Ahmed, M. K. Ahmed, M. Afifi, K. R. Shoueir and A. Abu-Rayyan, The degradation of methylene blue dye using copper-doped hydroxyapatite encapsulated into polycaprolactone nanofibrous membranes, *New J. Chem.*, 2021, **45**, 16143–16154.

28 Y. Kuang, X. Zhang and S. Zhou, Adsorption of methylene blue in water onto activated carbon by surfactant modification, *Water*, 2020, **12**, 1–19.

29 F. Krika and O. e. F. Benlahbib, Removal of methyl orange from aqueous solution via adsorption on cork as a natural and low-coast adsorbent: equilibrium, kinetic and thermodynamic study of removal process, *Desalin. Water Treat.*, 2015, **53**, 3711–3723.

30 M. D. Huff and J. W. Lee, Biochar-surface oxygenation with hydrogen peroxide, *J. Environ. Manage.*, 2016, **165**, 17–21.

31 P. Senthil Kumar, P. S. A. Fernando, R. T. Ahmed, R. Srinath, M. Priyadharshini, A. M. Vignesh and A. Thanjiappan, Effect of Temperature on the Adsorption of Methylene Blue Dye Onto Sulfuric Acid–Treated Orange Peel, *Chem. Eng. Commun.*, 2014, **201**, 1526–1547.

32 J. Cheng, C. Zhan, J. Wu, Z. Cui, J. Si, Q. Wang, X. Peng and L. S. Turng, Highly Efficient Removal of Methylene Blue Dye from an Aqueous Solution Using Cellulose Acetate

Nanofibrous Membranes Modified by Polydopamine, *ACS Omega*, 2020, **5**, 5389–5400.

33 J. Wang, J. Ma and Y. Sun, Adsorption of Methylene Blue by Coal-Based Activated Carbon in High-Salt Wastewater, *Water*, 2022, **14**, 1–18.

34 M. Abbasi, M. M. Sabzehmeidani, M. Ghaedi, R. Jannesar and A. Shokrollahi, Facile fabrication of leaf coral-like structured Cu-Al LDH/PVDF composite adsorptive membrane with enhanced adsorption performance, *Mater. Sci. Eng. B*, 2021, **267**, 115086.

35 P. Haroonian, M. Ghaedi, H. Javadian, C. Belviso and M. Abbasi, Simultaneous removal of tartrazine and erythrosine B using MnFe-layered double hydroxide nanoparticles modified PVDF polymer membrane, *Microporous Mesoporous Mater.*, 2025, **389**, 113569.

36 I. S. Aldabagh, D. Neithal and E. I. Ahmed, Removal of methylene blue from aqueous solution by green Synthesized silicon dioxide Nanoparticles using Sunflower Husk, *Chem. Eng. J. Adv.*, 2024, **18**, 100608.

37 T. R. do Nascimento Moraes Calazans, A. C. de Lima Barizão, T. de Andrade Silva, F. V. Campos, S. T. A. Cassini, A. V. F. Nardy Ribeiro, M. de Godoi Pereira, M. C. Cunegundes Guimarães, J. P. de Oliveira and J. N. Ribeiro, Methylene blue removal using a nanomagnetic support: a response surface approach, *Nanoscale Adv.*, 2024, **6**, 3887–3894.

38 D. Masekela, N. C. Hintsho-Mbita, B. Ntsendwana and N. Mabuba, Thin Films (FTO/BaTiO3/AgNPs) for Enhanced Piezo-Photocatalytic Degradation of Methylene Blue and Ciprofloxacin in Wastewater, *ACS Omega*, 2022, **7**, 24329–24343.

39 A. H. Jawad, A. S. Abdulhameed and M. S. Mastuli, Acid-factionalized biomass material for methylene blue dye removal: a comprehensive adsorption and mechanism study, *J. Taibah Univ. Sci.*, 2020, **14**, 305–313.

40 A. Kumar and R. Kataria, MOFs as versatile scaffolds to explore environmental contaminants based on their luminescence bustle, *Sci. Total Environ.*, 2024, **926**, 172129.

41 O. Rahmanian, M. Falsafin and M. Dinari, High surface area benzimidazole based porous covalent organic framework for removal of methylene blue from aqueous solutions, *Polym. Int.*, 2020, **69**, 712–718.

42 S. S. Paclijan, S. M. B. Franco, R. B. Abella, J. C. H. Lague and N. P. B. Tan, Fresh and Uncalcined Solution Blow Spinning - Spun PAN and PVDF Nanofiber Membranes for Methylene Blue Dye Removal in Water, *J. Membr. Sci. Res.*, 2021, **7**, 173–184.

43 Y. Chen, Y. Ma, W. Lu, Y. Guo, Y. Zhu, H. Lu and Y. Song, Environmentally friendly gelatin/β-cyclodextrin composite fiber adsorbents for the efficient removal of dyes from wastewater, *Molecules*, 2018, **23**(10), 2473.

44 E. Moradi, H. Ebrahimzadeh, Z. Mehrani and A. A. Asgharinezhad, The efficient removal of methylene blue from water samples using three-dimensional poly (vinyl alcohol)/starch nanofiber membrane as a green nanosorbent, *Environ. Sci. Pollut. Res.*, 2019, **26**, 35071–35081.

45 J. H. Li, H. Zheng, H. X. Lin, B. X. Zhang, J. Bin Wang, T. L. Li and Q. Q. Zhang, Preparation of Three Dimensional Hydroxyapatite Nanoparticles/Poly(vinylidene fluoride) Blend Membranes with Excellent Dye Removal Efficiency and Investigation of Adsorption Mechanism, *Chinese J. Polym. Sci.*, 2019, **37**, 1234–1247.

46 S. Haider, F. F. Binagag, A. Haider, A. Mahmood, N. Shah, W. A. Al-Masry, S. U. D. Khan and S. M. Ramay, Adsorption kinetic and isotherm of methylene blue, safranin T and rhodamine B onto electrospun ethylenediamine-grafted-polyacrylonitrile nanofibers membrane, *Desalin. Water Treat.*, 2015, **55**, 1609–1619.

47 P. Fagundes, T. K. Carniel, L. R. Mazon, J. M. M. de Mello, L. L. Silva, F. Dalcanton, G. L. Colpani, M. Zanetti and M. A. Fiori, Antimicrobial activity of the sodium lauryl sulphate used as surfactant in the polymeric encapsulation processes, *Mater. Sci. Forum*, 2020, **1012 MSF**, 500–505.

48 N. A. Falk, Surfactants as Antimicrobials: A Brief Overview of Microbial Interfacial Chemistry and Surfactant Antimicrobial Activity, *J. Surfactants Deterg.*, 2019, **22**, 1119–1127.

49 M. Wu, Z. Zhang, Z. Liu, J. Zhang, Y. Zhang, Y. Ding, T. Huang, D. Xiang, Z. Wang, Y. Dai, X. Wan, S. Wang, H. Qian, Q. Sun and L. Li, Piezoelectric nanocomposites for sonodynamic bacterial elimination and wound healing, *Nano Today*, 2021, **37**, 101104.

50 J. Wang, Z. Wen, Y. Xu, X. Ning, D. Wang, J. Cao and Y. Feng, Procedural Promotion of Wound Healing by Graphene-Barium Titanate Nanosystem with White Light Irradiation, *Int. J. Nanomedicine*, 2023, **18**, 4507–4520.

51 A. Ghazzy, R. R. Naik and A. K. Shakya, Metal–Polymer Nanocomposites: A Promising Approach to Antibacterial Materials, *Polymers*, 2023, **15**, 1–30.

52 U. Prakash Pamula, P. Yarasani, N. Rao Tentu and P. Ganji, Synthesis and Characterization of ZnO@CTAB-SA Polymer Nanocomposites with Biological and Photocatalytic Activity, *Front. Nanotechnol.*, 2025, **7**, 1–16.